
RELIOCC: Towards Reliable Semantic Occupancy Prediction via Uncertainty Learning

Song Wang¹, Zhongdao Wang², Jiawei Yu¹, Wentong Li¹,
Bailan Feng², Junbo Chen³, Jianke Zhu^{1*}
¹Zhejiang University ²Huawei Noah's Ark Lab ³Udeer.ai

Abstract

Vision-centric semantic occupancy prediction plays a crucial role in autonomous driving, which requires accurate and reliable predictions from low-cost sensors. Although having notably narrowed the accuracy gap with LiDAR, there is still few research effort to explore the reliability in predicting semantic occupancy from camera. In this paper, we conduct a comprehensive evaluation of existing semantic occupancy prediction models from a reliability perspective for the first time. Despite the gradual alignment of camera-based models with LiDAR in term of accuracy, a significant reliability gap persists. To addresses this concern, we propose RELIOCC, a method designed to enhance the reliability of camera-based occupancy networks. RELIOCC provides a plug-and-play scheme for existing models, which integrates hybrid uncertainty from individual voxels with sampling-based noise and relative voxels through mix-up learning. Besides, an uncertainty-aware calibration strategy is devised to further enhance model reliability in offline mode. Extensive experiments under various settings demonstrate that RELIOCC significantly enhances model reliability while maintaining the accuracy of both geometric and semantic predictions. Importantly, our proposed approach exhibits robustness to sensor failures and out of domain noises during inference.

1 Introduction

The goal of semantic occupancy prediction is to obtain a comprehensive voxel-based representation of the 3D scene from either LiDAR point clouds [1, 2] or camera images [3, 4, 5], which is crucial for the perception systems in autonomous driving and robotics. Initially, LiDAR-based models [1, 6, 7, 2] dominated the field due to their ability to provide accurate geometric cues. Researchers nowadays prefer to learn 3D occupancy information from images owing to the low cost and widespread availability of camera sensors. Recent progress [3, 4, 5, 8, 9] has significantly narrowed the gap in accuracy between camera and LiDAR-based approaches. However, their performance in terms of reliability remains under-explored, which becomes paramount in safety-critical scenarios.

Traditionally, the occupancy labeling relies on accumulated LiDAR point cloud and its corresponding 3D semantic labels [10, 11, 12, 13]. With the development of vision-centric approaches [3, 4, 8, 5, 9] using images, questions arise regarding the reliability of predictions solely derived from cameras without accurate depth information. Since the overall accuracy of occupancy networks is relatively low, exploring the reliability and uncertainty of their predictions can provide valuable reference information for downstream tasks, such as decision-making and planning [14, 15, 16].

With the above considerations, we conduct a thorough evaluation of existing semantic occupancy prediction models based on a reliability standpoint. To achieve this, we introduce the misclassification detection and calibration metrics from both geometric and semantic dimensions for evaluating model

*Corresponding author.

that utilize camera or LiDAR data. Our findings reveal that, camera-based models often lag behind their LiDAR-based counterparts in terms of reliability despite improvements in accuracy.

To mitigate this disparity, RELIOCC is proposed to improve the reliability in occupancy networks via a new hybrid uncertainty learning scheme. Our approach optimizes uncertainty by taking into account of perturbations in individual voxels (*absolute uncertainty*) and the relative relationships in mix-up voxels (*relative uncertainty*) during model training. By integrating multiple sources of information for uncertainty learning, our method enhances the reliability of camera-based models without sacrificing inference speed or accuracy. Moreover, we provide an uncertainty-aware calibration strategy to utilize the learned uncertainty in offline mode, further enhancing model reliability. Through extensive experiments across diverse configurations including online and offline modes, our method achieves competitive performance compared against the state-of-the-art models.

Our main contributions can be summarized as follows:

- A comprehensive evaluation is conducted on existing semantic occupancy prediction models from a reliability perspective, which provides a series of misclassification detection and calibration metrics across both geometric and semantic dimensions.
- To adapt the existing methods for occupancy networks, we propose the RELIOCC to enhance the reliability of camera models. A novel hybrid uncertainty learning approach is presented to combine the variance from individual and mix-up voxels and significantly narrow the reliability gap between camera and LiDAR-based methods.
- Extensive experiments on online uncertainty learning and offline model calibration under various settings, demonstrate the effectiveness of our approach on general condition and robustness in adverse condition like sensor failures and noisy observations.

2 Preliminaries

2.1 Problem Formulation

Occupancy Prediction. Given inputs \mathbf{x} from LiDAR or camera sensors, occupancy networks $V_\theta(\mathbf{x})$ generate dense features $\mathcal{V} \in \mathbb{R}^{d \times L \times W \times H}$ in a pre-defined volume, where L , W , and H represent the length, width, and height, respectively. d is the dimension of dense features. For any voxel $v_i \in \mathbb{R}^d$ within this volume, the prediction involves with two components. One is a binary indicator that specifies whether the voxel is occupied or not. The other is the semantic label of the voxel if the voxel is occupied. Generally, such process can be formulated by estimating the probability $p(y_i = y | v_i)$ for v_i , where $y \in \{0, 1, \dots, S\}$. Here, 0 denotes that the voxel is unoccupied, and S is the total number of semantic classes.

Misclassification Detection. For a reliable classifier, we expect it to accurately reject those incorrect predictions with low-confidence. Misclassification detection is introduced to measure the gap between the actual trained model and the ideal one, which can be evaluated by *rejection curves* [17, 18]. To avoid the tendency of higher precision models, we adopt the same strategy as [19, 20] to normalize the area under the curve and deducts a baseline score.

Calibration. As a long-standing problem in machine learning, the goal of model calibration is to ensure that predicted confidence of a model aligns accurately with the actual likelihood of correctness [21, 22], thereby producing more reliable predictions. Within the framework of multi-class classification, a model is deemed perfectly calibrated if $p(y_i = y | c_i = c, v_i) = c$. Here, the model not only predicts a discrete label y but also generates a confidence score $c \in [0, 1]$. This score c should ideally reflect the true probability that the predictions are correct.

2.2 Evaluation Metrics

Canonical Metrics. Following common practice [23, 10], we employ the Intersection over Union (IoU) metric to assess the accuracy of geometric occupancy prediction that is typically treated as a binary classification task. Additionally, we utilize the mean Intersection over Union (mIoU) across multiple categories to evaluate the quality of semantic predictions. These two metrics are calculated using discrete predictions by applying argmax operation to the logits. Although IoU and mIoU effectively reflect the performance of model in accuracy, they do not assess its reliability.

In this paper, we mainly evaluate the reliability of occupancy prediction on two aspects including misclassification detection and calibration, which are assessed with following metrics.

Prediction Rejection Ratio (PRR). The Prediction Rejection Ratio (PRR) [19] is defined through *rejection curves* for misclassification detection. To construct a rejection curve, we initially sort predictions based on a specific criterion, such as predicted confidence or oracle confidence (where predictions are labeled 1 if correct and 0 otherwise). Subsequently, a threshold is set and predictions below this threshold are rejected, allowing us to calculate a rejection rate. As this threshold is incrementally adjusted, we obtain a rejection curve to illustrate how the classification error (depicted on the y -axis) decreases in tandem with the rejection rate (represented on the x -axis). The PRR metric is then quantitatively defined as follows

$$\text{PRR} = \frac{AUC_{\text{random}} - AUC_{\text{uncertainty}}}{AUC_{\text{random}} - AUC_{\text{oracle}}}, \quad (1)$$

where AUC represents the Area Under the Curve. Here, $AUC_{\text{random}} = 0.5$ corresponds to the AUC for randomly generated confidences. A perfectly reliable model would achieve a $\text{PRR} = 1$. For occupancy networks, we report both PRR_{geo} for geometric predictions and PRR_{sem} for semantic predictions, respectively.

Expected Calibration Error (ECE). Expected Calibration Error (ECE) [24, 22] assesses the calibration of probabilistic predictions made by machine learning models. It measures the difference between predicted probabilities and observed frequencies across various confidence levels. Intuitively,

$$e_{\text{ECE}} = \mathbb{E}_{\hat{c}_i} [| p(\hat{y}_i = y_i | \hat{c}_i = c) - c |]. \quad (2)$$

A perfectly calibrated model yields $e_{\text{ECE}} = 0$. Eq. (2) is a continuous integration over $c \in [0, 1]$. Practically, we approximate this integration by discretizing c into M small bins. Denoting the set of samples falling into the m -th bin as B_m , the expectation can be calculated as

$$\text{ECE} = \sum_{m=1}^M \frac{|B_m|}{N} | \text{acc}(B_m) - \text{conf}(B_m) |, \quad (3)$$

where $\text{acc}(\cdot)$ denotes the mean accuracy, and $\text{conf}(\cdot)$ is mean confidence of B_m . N is the number of samples. We set the number of bins $M = 15$ by default. As with PRR, we report both ECE_{geo} and ECE_{sem} for geometric and semantic predictions, respectively.

3 Adaptation with Existing Methods for Occupancy Networks

Reliable predictions are paramount in occupancy networks, especially in critical applications such as autonomous driving and robotics where safety is a strict requirement. Despite their importance, methods for enhancing the reliability of occupancy networks are still under-explored in the existing literature. To address this gap, we begin by reviewing existing uncertainty learning and calibration methods, which are mostly developed to improve the reliability for traditional tasks. Then, we adapt them for the recent occupancy networks.

We categorize these methods into two paradigms. One is training uncertainty predictor $c_{\sigma|\phi}$ based on the dense features \mathcal{V} concurrently with V_θ from scratch, which is termed *online uncertainty learning*. Another is training scaling factor $c_{f|\phi}$ on top of a fixed V_θ , which is termed *offline model calibration*. In the experimental section (see §5.1 and §5.2), we provide extensive evaluations on these methods to compare their effectiveness in boosting the reliability of occupancy networks.

3.1 Online Uncertainty Learning

Uncertainty estimation is a long-standing problem in the context of Bayesian deep learning [25, 26, 27]. Prior arts can be classified into ones concerning epistemic (model) uncertainty [28, 29] and ones concerning aleatoric (data) uncertainty [30, 31]. Although explicit uncertainty estimates are obtainable, we do not directly evaluate these estimates in online mode. Instead, since the uncertainty is learned concurrently with the model’s predictions from scratch, we use them as a regularization term of helping the model become more reliable.

For each voxel feature \mathbf{v}_i , we compute a logit vector $\mathbf{z}_i \in \mathbb{R}^{S+1}$ using a linear layer, where S represents the number of semantic classes.

Heteroscedastic Aleatoric Uncertainty (HAU) [31] is a data-dependent uncertainty learning method. We employ the classification form of HAU, which modifies upon a deterministic model by placing a Gaussian over the logit: $\hat{\mathbf{z}}_i|\phi \sim \mathcal{N}(\mathbf{z}_i, (\sigma_i^\phi)^2)^2$. The sampled logit vector $\hat{\mathbf{z}}_i$ is then passed through a *softmax* operator and cross entropy loss is computed. Here σ_i^ϕ is the predicted uncertainty parameterized by ϕ . Optimization of ϕ can be done with back-propagation using the re-parameterization trick [32]: $\hat{\mathbf{z}}_i = \mathbf{z}_i + \sigma_i^\phi \epsilon, \epsilon \in \mathcal{N}(\mathbf{0}, \mathbf{I})$. Note that the uncertainty predictions vary for different voxel i .

Data Uncertainty Learning (DUL) [33] shares a similar spirit with HAU with two distinctions. Instead of using the logit $\hat{\mathbf{z}}_i$, DUL models the feature $\hat{\mathbf{v}}_i$ as a Gaussian distribution by $\hat{\mathbf{v}}_i = \mathbf{v}_i + \sigma_i^{\mathbf{W}} \epsilon$. Moreover, DUL introduces a regularization term in the loss function that minimizes the Kullback–Leibler (KL) divergence between the predicted Gaussian and a standard Gaussian.

MC Dropout (MCD) [29] is proposed to explore the epistemic (model) uncertainty. Differently from the above methods, MCD does not require additional parameters to learn uncertainty. Instead, it incorporates multiple dropout layers into the original network during training. For inference, the occupancy prediction of each voxel is obtained by $\hat{\mathbf{z}}_i = \frac{1}{K} \sum_{k=1}^K \mathbf{z}_{k,i}$, where $\mathbf{z}_{k,i}$ is the model output at the k -th test. The normalized entropy of K predictions is adopted as the model uncertainty. To fully explore the uncertainty within the model, we set $K = 40$ in our experiments.

For above online uncertainty learning methods, the calibrated confidence is set as the *softmax* output of the sampled logit and then determined by taking the maximum probability across all classes: $c_i = \max_s \mathcal{S}(\hat{\mathbf{z}}_i)^{(s)}$, where \mathcal{S} denotes the *softmax* function.

3.2 Offline Model Calibration

Offline calibration methods build on pre-trained V_θ and need to learn a scaling function, which typically employ the following formulation

$$c_i \equiv c_{f|\phi}(\mathbf{z}_i) = \max_s f_\phi(\mathbf{z}_i)^{(s)}, \quad (4)$$

where f_ϕ is the scaling function applied to \mathbf{z}_i parameterized by the learnable parameters ϕ . In the absence of explicit uncertainty estimation, uncertainty σ_i is set to $1 - c_i$.

Temperature Scaling (TempS) [22] employs a scalar parameter T , termed as temperature, to scale the logits \mathbf{z}_i , by $f_\phi(\mathbf{z}_i) = \mathcal{S}(\frac{\mathbf{z}_i}{T})$. T is data-independent, which is shared across all classes.

Dirichlet Scaling (DiriS) [34] assumes that the model’s output follow a Dirichlet distribution. Based on this assumption, they propose the Dirichlet scaling, $f_\phi(\mathbf{z}_i) = \mathcal{S}(\mathbf{W} \cdot \log(\mathcal{S}(\mathbf{z}_i)) + \mathbf{b})$. Here, learnable parameters ϕ includes weight $\mathbf{W} \in \mathbb{R}^{(S+1) \times (S+1)}$ and bias $\mathbf{b} \in \mathbb{R}^{S+1}$.

Meta-Calibration (MetaC) [35] proposes to use the entropy of model prediction $-c_i \log(c_i)$ to select different calibrators. Specifically, an identical $f_\phi(\mathbf{z}_i) = \mathcal{S}(\frac{\mathbf{z}_i}{T})$ as in TempS is used when $-c_i \log(c_i)$ is smaller than the predefined threshold η . Otherwise, the calibration function $f_\phi(\mathbf{z}_i)$ is set to the constant value $\frac{1}{S+1}$. MetaC introduces new randomness into predictions, which leads to variations in accuracy, making it less practical for safety-critical tasks such as occupancy prediction.

Depth-Aware Scaling (DeptS) [36] is an improved variant upon MetaC, which is specially designed for LiDAR segmentation. Depth d_i of each point or voxel is encoded into the calibration function f_ϕ by a linear mapping $\alpha_i = k_1 \cdot d_i + k_2$, where k_1 and k_2 are learnable parameters. When prediction entropy $-c_i \log(c_i)$ is greater than the threshold η , $f_\phi(\mathbf{z}_i) = \mathcal{S}(\frac{\mathbf{z}_i}{\alpha \cdot T_1})$. Otherwise, $f_\phi(\mathbf{z}_i) = \mathcal{S}(\frac{\mathbf{z}_i}{\alpha \cdot T_2})$. Both T_1 and T_2 are temperature parameters, where T_1 is initially set higher than T_2 .

4 RELIOCC

Method Overview. Inspired by investigation on prior arts, we propose RELIOCC, a plug-and-play method tailored for the 3D occupancy prediction task. RELIOCC has two main improvements over existing methods. Firstly, beyond traditional uncertainty learning, we propose to utilize the relative relationships between voxel pairs of uncertainty estimates in order to further refine the uncertainty

²We omit predicting the mean $\mu^\phi(\mathbf{z}_i)$ and use \mathbf{z}_i for simplicity. Empirical results are similar.

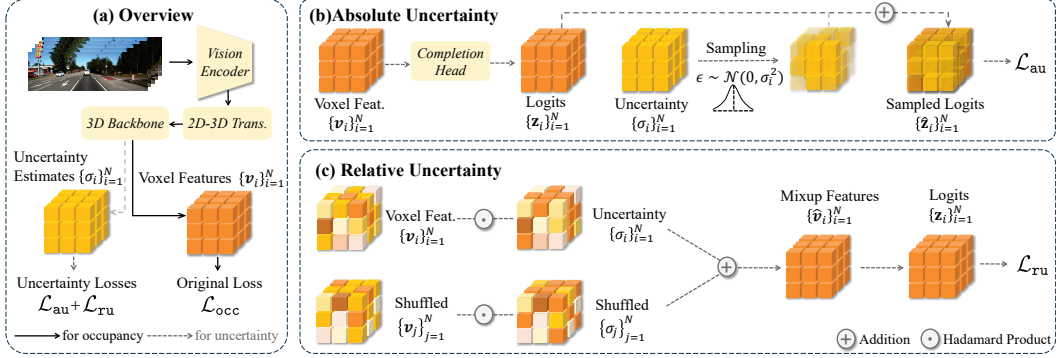


Figure 1: (a) *Overview of proposed RELIOCC.* Besides the original objective of an occupancy network, we introduce an uncertainty estimation branch and supervise it with absolute and relative uncertainty learning losses. (b) *Absolute uncertainty learning.* Deterministic logits are replaced with ones sampled from predicted distributions. (c) *Relative uncertainty learning.* We leverage the relative relationships between uncertainty pairs to further enhance uncertainty learning.

estimation process. Secondly, we present a unified framework that integrates the methodologies of uncertainty learning with scaling-based calibration, which demonstrates that their synergy offers substantial benefits. As shown in Figure 1(a), we predict a scalar uncertainty σ_i from a voxel feature v_i using an MLP, which receives supervision from both the individual and relative voxels.

Absolute Uncertainty. By *absolute* here we mean the uncertainty σ_i is only determined by the individual v_i itself while ignoring relative relations between a pair of v_i and v_j . For absolute uncertainty, we adopt a similar formulation as in HAU [31]. Specifically, We randomly sample the logit \hat{z}_i based on the predicted uncertainty σ_i by $\hat{z}_i = z_i + \sigma_i \epsilon$, $\epsilon \in \mathcal{N}(\mathbf{0}, \mathbf{I})$ as illustrated in Figure 1(b). We denote this absolute uncertainty loss as \mathcal{L}_{au} , which is computed with the re-sampled logit \hat{z}_i and its corresponding ground truth.

Relative Uncertainty. A potential drawback of absolute uncertainty is that the optimization of σ_i tends to plateau once it reaches a small scale. To address this issue, we introduce the concept of relative uncertainty learning for occupancy prediction. The fundamental principle of relative uncertainty learning involves enforcing comparisons between uncertainty pairs v_i and v_j . This approach ensures that optimization does not plateau, even when σ_i and σ_j are small.

Concretely, we shuffle voxel features in \mathcal{V} , paired the shuffled features with the original ones and obtain random pairs (v_i, v_j) at each iteration. Inspired by the mix-up [37] learning principle, we blend the paired voxel features with $\hat{v} = \lambda v_i + (1 - \lambda)v_j$. Correspondingly \hat{v} is trained with a blend of the label pairs using cross-entropy loss. The blended label $y = y_i + y_j$, where y_i, y_j are one-hot label encodings³. We employ the predicted uncertainty for the weighting: $\lambda = \frac{\sigma_i}{\sigma_i + \sigma_j} \in [0, 1]$. We denote the loss computed with blended label and mixed output from the shared completion head as the relative uncertainty loss \mathcal{L}_{ru} , as shown in Figure 1(c).

An intuitive understanding emerges when considering that relative uncertainty adaptively modulates the learning dynamics between the feature pair (v_i, v_j) . Specifically, if the model exhibits greater confidence in the prediction associated with v_i , it suffices for the mixup feature to incorporate a smaller portion of v_i while still achieving a reduced loss \mathcal{L}_{ru} . In contrast, a lower confidence in v_j necessitates a greater inclusion of v_j within the mixup to diminish the loss. Consequently, this process enables the model to effectively differentiate between the uncertainties σ_i and σ_j , typically resulting in a smaller σ_i and a larger σ_j . Importantly, this differentiation does not hinge on the absolute magnitudes of $\sigma_{i,j}$. Rather, it is the relative relationship between them that is central to the learning process. In driving scenarios, there are rich relative relationships between voxels, including *distance*, *occupancy*, *surface* and *interior* properties. This focus on relative differences ensures that the model’s adjustments are robust to the absolute scales of the uncertainties.

Uncertainty-Aware Calibration. Using the above two uncertainty estimation objective, RELIOCC is capable of learning uncertainty with existing occupancy models in an online setting. We introduce a scaling-based calibration objective to make it also compatible with the offline setting. A variant

³Different from the original mix-up [37] paper, we omit weighting the labels with λ for stable training.

Table 1: The accuracy and reliability evaluation of state-of-the-art semantic occupancy prediction models on the validation set of SemanticKITTI [10]. * indicates that the output of SCPNet is a sparse representation and does not contain confidence score for empty voxels, making it infeasible to evaluate the corresponding geometric metrics in reliability.

Method	Modality	Semantics			Geometry		
		mIoU (%) \uparrow	PRR _{sem} (%) \uparrow	ECE _{sem} (%) \downarrow	IoU(%) \uparrow	PRR _{geo} (%) \uparrow	ECE _{geo} (%) \downarrow
SSCNet _[CVPR17] [23]	LiDAR	16.41	46.77	1.61	50.75	42.92	0.97
LMSCNet _[3DV20] [1]	LiDAR	17.27	48.89	0.79	54.91	48.01	0.67
JS3C-Net _[AAAI21] [23]	LiDAR	22.77	41.09	2.94	53.08	37.04	1.64
SSC-RS _[IJROS23] [39]	LiDAR	24.75	45.04	0.87	58.62	44.29	0.72
SCPNet* _[CVPR23] [2]	LiDAR	35.06	38.35	2.52	49.06	-	-
MonoScene _[CVPR22] [3]	Camera	11.30	41.95	6.65	36.79	38.39	5.95
TPVFormer _[CVPR23] [4]	Camera	11.30	38.83	7.10	35.62	32.10	6.32
NDCScene _[ICCV23] [8]	Camera	12.70	43.29	7.24	37.24	40.17	6.45
VoxFormer _[CVPR23] [5]	Camera	13.17	42.97	5.90	43.96	36.56	5.02
SGN _[arXiv23] [9]	Camera	15.52	44.72	5.69	45.45	39.78	4.85

form of TempS [22] is adopted, and the uncertainty-aware temperature T_σ is a linear transform of σ_i :

$$T_\sigma = k_1 \cdot \sigma_i + k_2, \quad f_\phi(\mathbf{z}_i) = \mathcal{S} \left(\frac{\mathbf{W} \cdot \mathbf{z}_i + \mathbf{b}}{T_\sigma} \right), \quad (5)$$

where k_1 and k_2 are learnable parameters, and \mathbf{b} is the bias. \mathbf{W} is initialized as the identity matrix and only the elements on the diagonal are optimized. The calibration loss is denoted as $\mathcal{L}_{\text{calib}}$.

Training and Inference. RELIOCC supports both online uncertainty learning and offline model calibration settings. In the online setting, the uncertainty predictor is trained concurrently with the occupancy network from scratch. The total loss function comprises \mathcal{L}_{occ} , \mathcal{L}_{au} , and \mathcal{L}_{ru} . Here, \mathcal{L}_{occ} represents the primary loss for the occupancy network. During inference, the model operates consistently with the original design as the predicted uncertainties are not utilized. In the offline setting, the occupancy network is fixed, eliminating the need for \mathcal{L}_{occ} and introducing the calibration loss $\mathcal{L}_{\text{calib}}$ instead. The inference process incurs a minimal increase in computational overhead due to the addition of the calibrator.

5 Experiments

Datasets and Evaluation. SemanticKITTI [10] is the first large-scale outdoor dataset for semantic occupancy prediction containing 64-beam LiDAR point clouds and camera images as inputs [38]. The dataset comprises 22 sequences, where 00-10 (excluding 08) are used as the training set, 08 is the validation set, and 11-21 are the test set. Since the ground truth for the test set is not publicly available, we cannot measure our newly introduced metrics on it. Therefore, we primarily evaluate existing methods on the validation set (val.). As described in §2.2, mIoU and IoU are used to measure the model’s accuracy in semantic and geometric completion, respectively. For misclassification detection and calibration metrics including PRR and ECE, we also report the corresponding results from both geometric and semantic perspectives.

Re-evaluated Methods. We reproduce and evaluate existing publicly available methods on the SemanticKITTI benchmark, including five LiDAR-based models [23, 1, 7, 39, 2] and five camera-based models [3, 4, 5, 8, 9]. All results are obtained using the official implementation and the configurations are kept consistent for inference, with relevant links provided in our supplemental material. As shown in Tab. 1, we find that although the accuracy of camera-based methods has been continuously improved and gradually approaches the baseline accuracy of LiDAR methods, their reliability metrics, particularly the ECE, have not shown corresponding improvements. In cases of lower accuracy compared to LiDAR, the camera-based models’ reliability is also quite poor, which undoubtedly poses significant safety risks for autonomous driving.

5.1 Online Uncertainty Learning

Base Architectures and Competing Methods. Considering the potential applications of camera-based methods and their current limitations, we adopt the state-of-the-art vision-based methods including VoxFormer [5] and SGN [9] as our base architectures to conduct relevant experiments. For the online uncertainty learning, we report the results of some existing methods on the two baseline frameworks for comparison, including HAU [31], DUL [33], and MCD [29] (see §3.1).

Table 2: Quantitative results of online uncertainty learning (§5.1) on SemanticKITTI [10] (val.).

Method	Semantics			Geometry		
	mIoU (%) \uparrow	PRR _{sem} (%) \uparrow	ECE _{sem} (%) \downarrow	IoU(%) \uparrow	PRR _{geo} (%) \uparrow	ECE _{geo} (%) \downarrow
<i>VoxFormer Framework</i>						
VoxFormer [CVPR23] [5]	13.17	42.97	5.90	43.96	36.56	5.02
VoxFormer+HAU [NIPS17] [31]	13.43	45.38	5.26	43.57	40.72	4.47
VoxFormer+DUL [CVPR20] [33]	13.29	43.57	6.09	44.10	38.66	5.17
VoxFormer+MCD [MICCAI19] [29]	13.28	42.21	5.83	43.90	37.43	4.99
VoxFormer+RELI OCC (Ours)	13.43	47.75	2.84	43.28	44.58	2.57
<i>SGN Framework</i>						
SGN [arXiv23] [9]	15.52	44.72	5.69	45.45	39.78	4.85
SGN+HAU [NIPS17] [31]	15.50	46.51	5.08	45.07	44.24	4.34
SGN+DUL [CVPR20] [33]	15.81	44.00	5.78	45.75	39.56	4.95
SGN+MCD [MICCAI19] [29]	15.62	44.70	6.02	45.50	40.34	5.11
SGN+RELI OCC (Ours)	15.65	50.72	3.75	45.78	49.61	3.07

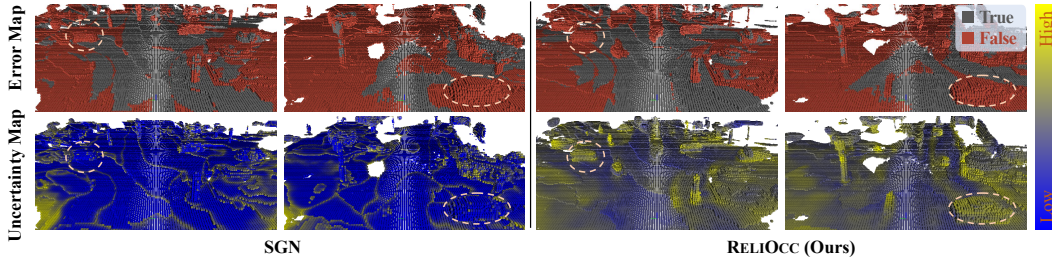


Figure 2: Visual results of the error map and uncertainty map from the prediction by SGN [9] and RELIOCC. In the uncertainty map, a closer proximity to *yellow* indicates a higher level of uncertainty.

Implementation Details. We follow the original training setting and add additional uncertainty learning parameters without altering the network structure. The inputs consist of the current image from the left camera and previous 4 frames. The image size is copped into 1220×370 . VoxFormer [5] and SGN [9] with online uncertainty estimation are trained for 20 epochs and 40 epochs, respectively. The loss coefficients (α, β) for \mathcal{L}_{au} and \mathcal{L}_{ru} are set to (4.0, 6.0) for both frameworks. All the experiments are conducted on 8 NVIDIA Tesla V100 GPUs within the same experimental environment. Further implementation details can be found in the supplemental material.

Quantitative Results. In Tab. 2, we provide the comparison among the methods with the same framework for fairness. Compared to data uncertainty-based HAU [31] and DUL [33], as well as model uncertainty-based MCD [29], our method shows significant improvements in the new evaluation metrics for reliability. The calibration errors (ECE) in both semantic and geometric aspects are significantly reduced compared to the existing uncertainty estimation methods. The improvement in PRR also indicates a notable enhancement in model reliability. Our method maintains stability in terms of the original accuracy (mIoU and IoU) across the two different frameworks.

Qualitative Results. To further verify the effect of our method, we visualize the error map with corresponding uncertainty map of SGN [9] and our approach. The uncertainty for vanilla SGN is obtained by subtracting the confidence from 1. As shown in Figure 2, when the network’s predictions exhibit large areas of error, SGN’s uncertainty map still shows low uncertainty, indicating high confidence in prediction. In contrast, our proposed RELIOCC displays high uncertainty in most of the error regions, providing more reliable information for downstream tasks.

5.2 Offline Model Calibration

In this section, VoxFormer and SGN are also adopted as baseline frameworks. We primarily compare our method with scaling-based model calibration approaches including TempS [22], DiriS [34], MetaC [35], and DeptS [36] (see §3.2).

Implementation Details. We select the best-performing model checkpoints on the validation set from the pre-trained VoxFormer and SGN as the targets for calibration. During the calibration process, the parameters of the original network are frozen, and only the parameters ϕ in the calibration function f_ϕ and uncertainty learning layers are trainable. For both frameworks, these methods are trained on 8 GPUs for 20 epochs with a learning rate as 0.001 and AdamW optimizer [40]. The batch size is set to 1 per GPU. For our method, the loss weights (α, β, γ) for uncertainty learning ($\mathcal{L}_{\text{au}}, \mathcal{L}_{\text{ru}}$) and model calibration ($\mathcal{L}_{\text{calib}}$) are set to 1.5, 1.0, and 4.0, respectively.

Table 3: Quantitative results of offline model calibration (§5.2) on SemanticKITTI [10] (val.).

Method	Semantics			Geometry		
	mIoU(%) \uparrow	PRR _{sem} (%) \uparrow	ECE _{sem} (%) \downarrow	IoU(%) \uparrow	PRR _{geo} (%) \uparrow	ECE _{geo} (%) \downarrow
<i>VoxFormer Framework</i>						
VoxFormer [CVPR23] [5]	13.17	42.97	5.90	43.96	36.56	5.02
VoxFormer+TempS [ICML17] [22]	13.17	43.63	2.61	43.96	33.59	2.28
VoxFormer+DiriS [NeurIPS19] [34]	13.17	48.12	2.38	43.96	42.78	2.42
VoxFormer+MetaC [ICML21] [35]	11.86	43.06	4.11	34.73	34.80	3.67
VoxFormer+DeptS [arXiv24] [36]	13.17	41.29	2.27	43.96	30.31	1.63
VoxFormer+RELI OCC (Ours)	13.17	48.17	2.05	43.96	44.34	2.57
<i>SGN Framework</i>						
SGN [arXiv23] [9]	15.52	44.72	5.69	45.45	39.78	4.85
SGN+TempS [ICML17] [22]	15.52	46.90	2.68	45.45	37.25	2.35
SGN+DiriS [NeurIPS19] [34]	15.52	48.20	2.61	45.45	43.04	2.51
SGN+MetaC [ICML21] [35]	14.71	46.38	4.06	40.37	37.97	3.65
SGN+DeptS [arXiv24] [33]	15.52	45.45	2.14	45.45	34.99	1.42
SGN+RELI OCC (Ours)	15.52	47.40	2.09	45.45	43.80	2.43

Quantitative Results. As illustrated in Tab. 3, all model calibration methods demonstrate improvements compared to the baselines, particularly in calibration error (ECE). MetaC [35] loses the characteristic of maintaining accuracy in calibration due to the introduction of new random classifications. Our approach with uncertainty-aware design achieves competitive performance on both ECE and PRR metrics without depth information even compared with the state-of-the-art DeptS [36].

Qualitative Results. We visualize the semantic calibration gaps in SGN [9] and RELI OCC by reliability diagrams [41, 21], which plot the confidence of prediction with the corresponding voxel-wise accuracy. Our method shows significant improvement over the baseline model in calibration gaps, as indicated by the Gap areas between the predicted accuracy with the expected accuracy (smaller indicates better), as shown in the Figure 3. Additional reliability diagrams are provided in the supplemental material.

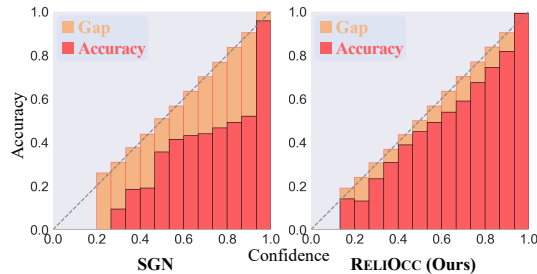


Figure 3: The reliability diagrams of semantic calibration gaps from SGN [9] and RELI OCC.

5.3 Diagnostic Experiments

To further validate the effectiveness of our approach, we present diagnostic experiments in this section. Due to page limitations, some experimental results are provided in the supplemental material.

Ablation of Online Uncertainty Learning. Table 4: Ablation of our online uncertainty learning.

We provide ablation experiments on the effect of absolute uncertainty and relative uncertainty during the whole model training. The experiments are conducted with Vox-

Absolute Unc.	Relative Unc.	PRR _{sem} \uparrow	ECE _{sem} \downarrow	PRR _{geo} \uparrow	ECE _{geo} \downarrow
		42.97	5.90	36.56	5.02
✓		45.47	5.41	41.54	4.62
	✓	46.58	4.02	42.65	4.31
✓	✓	47.75	2.84	44.58	2.57

Former [5] on the validation set of SemanticKITTI. As shown in Tab. 4, the first row presents the baseline results. The inclusion of individual absolute uncertainty and relative uncertainty both contribute to the improvement of the model’s reliability, although the improvement is relatively limited. When our proposed hybrid uncertainty learning module is incorporated, the PRR and ECE metrics of model’s prediction achieve the best results.

Ablation of Offline Model Cali-

bration. Further ablations are also conducted in offline mode. With the pre-trained VoxFormer, we found that employing standard scaling

Table 5: Ablation of our offline model calibration.

Scaling Calib.	Relative Unc.	Absolute Unc.	PRR _{sem} \uparrow	ECE _{sem} \downarrow	PRR _{geo} \uparrow	ECE _{geo} \downarrow
			42.97	5.90	36.56	5.02
✓			43.63	2.61	33.59	2.28
✓	✓		45.13	1.75	39.66	2.19
✓	✓	✓	48.17	2.05	44.34	2.57

strategies such as TempS [22] can achieve good calibration results as illustrated in second row of Tab. 5. However, it impacts the improvement of misclassification detection metrics (PRR) and even leads to a decline in geometry. Our introduced relative uncertainty learning can further improve calibration performance and enhance misclassification detection. Furthermore, the combination of absolute and relative uncertainties achieves the best performance in misclassification detection, although it is slightly less effective in calibration compared to using relative uncertainty alone.

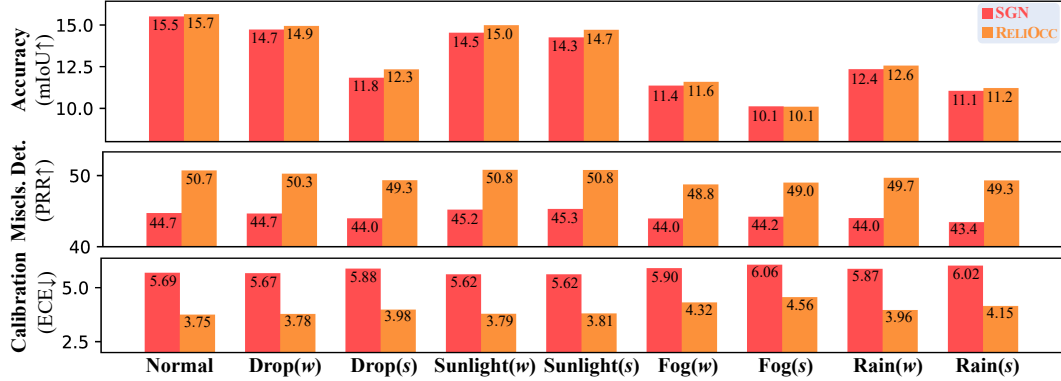


Figure 4: The comparison in accuracy and reliability performance between SGN [9] and RELIOCC under four out-of-domain conditions. Due to space constraints, we provide the semantic comparison here, while the geometric comparison is included in the supplemental material.

Robustness Analysis. Fig 4 presents the robustness analysis results of RELIOCC compared to the baseline model SGN [9]. We simulate four potential out-of-domain scenarios during the inference, including sensor failures (frames drop), strong sunlight, foggy and rainy conditions, to evaluate the model’s robustness [42]. Each adverse scenario provides *weak(w)* and *strong(s)* modes of perturbation. As the noise increases in various conditions, our method not only maintains stability in reliability metrics but also demonstrates more improvement in accuracy compared to the baseline.

6 Related Work

Semantic Occupancy Prediction. Semantic occupancy prediction (SOP) is also known as semantic scene completion (SSC) and firstly explored in indoor scenes [23, 43, 44, 45, 46]. In outdoor scenarios, SemanticKITTI [10] stands as the first large-scale dataset, providing abundant data resources. Recently, several other datasets [47, 12, 13, 11] have been constructed to explore this task owing to its importance. LiDAR-based methods [1, 48, 49, 50, 6, 7, 47, 2] have dominated this field in accuracy. MonoScene [3] is the first occupancy prediction method that utilizes single image as input. Subsequent studies [4, 5, 9, 51, 52, 53, 54, 55, 56, 57, 58, 59, 60, 61, 62, 63, 64] have effectively improved the performance of camera-based models. However, there is a lack of research on reliability of occupancy predictions, posing potential risks to the safety of downstream tasks in driving [14, 15, 16]. RELIOCC fills this gap by investigating the reliability of occupancy networks via uncertainty learning.

Uncertainty Learning and Model Calibration. The uncertainty in machine learning consists of aleatoric uncertainty from data noises and epistemic uncertainty from model parameters [31, 65]. Data uncertainty is widely explored in face field [33, 66, 67, 68, 69, 70]. Cai *et al.* [71] propose a probabilistic embedding model to estimates the data uncertainty for point cloud. Model uncertainty is usually obtained from the statistics of multiple predictions through methods including model ensembling [72], bootstrapping [73], and bagging [74]. Model calibration is another line to improving reliability in model prediction [20], which provides a post-processing scheme applied to the non-probabilistic output from a trained model. Model calibration was initially studied in image classification [22, 75, 34, 35] and has since been widely applied to object detection [76, 77, 78, 79] and semantic segmentation [80, 81, 82, 36]. Our method adopts uncertainty as a learning objective and can support both online uncertainty estimation and offline model calibration simultaneously.

7 Conclusion

In this paper, we address the issue of assessing reliability in semantic occupancy prediction for the first time. The reliability is evaluated from the two aspects including misclassification detection and calibration. Exhaustive evaluation of existing LiDAR and camera-based methods are provided. Besides, we propose a new scheme RELIOCC that integrates hybrid uncertainty from the individual and relative voxels into existing occupancy networks without affecting accuracy or inference speed. Both online and offline modes are designed to illustrate the generalization capability of our learned

uncertainty. Extensive experiments are conducted under various settings, demonstrating RELIOCC is effective in improving the reliability and robustness of semantic occupancy models.

References

- [1] Luis Roldao, Raoul de Charette, and Anne Verroust-Blondet. LMSCNet: Lightweight multiscale 3D semantic completion. In *3DV*, pages 111–119, 2020.
- [2] Zhaoyang Xia, Youquan Liu, Xin Li, Xinge Zhu, Yuexin Ma, Yikang Li, Yuenan Hou, and Yu Qiao. SCPNet: Semantic scene completion on point cloud. In *CVPR*, pages 17642–17651, 2023.
- [3] Anh-Quan Cao and Raoul de Charette. MonoScene: Monocular 3D semantic scene completion. In *CVPR*, pages 3991–4001, 2022.
- [4] Yuanhui Huang, Wenzhao Zheng, Yunpeng Zhang, Jie Zhou, and Jiwen Lu. Tri-perspective view for vision-based 3D semantic occupancy prediction. In *CVPR*, pages 9223–9232, 2023.
- [5] Yiming Li, Zhiding Yu, Christopher Choy, Chaowei Xiao, Jose M Alvarez, Sanja Fidler, Chen Feng, and Anima Anandkumar. VoxFormer: Sparse voxel transformer for camera-based 3D semantic scene completion. In *CVPR*, pages 9087–9098, 2023.
- [6] Ran Cheng, Christopher Agia, Yuan Ren, Xinhai Li, and Liu Bingbing. S3CNet: A sparse semantic scene completion network for LiDAR point cloud. In *CoRL*, pages 2148–2161, 2021.
- [7] Xu Yan, Jiantao Gao, Jie Li, Ruimao Zhang, Zhen Li, Rui Huang, and Shuguang Cui. Sparse single sweep LiDAR point cloud segmentation via learning contextual shape priors from scene completion. In *AAAI*, pages 3101–3109, 2021.
- [8] Jiawei Yao, Chuming Li, Keqiang Sun, Yingjie Cai, Hao Li, Wanli Ouyang, and Hongsheng Li. Ndc-scene: Boost monocular 3d semantic scene completion in normalized device coordinates space. In *ICCV*, pages 9455–9465, 2023.
- [9] Jianbiao Mei, Yu Yang, Mengmeng Wang, Junyu Zhu, Xiangrui Zhao, Jongwon Ra, Laijian Li, and Yong Liu. Camera-based 3d semantic scene completion with sparse guidance network. *arXiv preprint arXiv:2312.05752*, 2023.
- [10] Jens Behley, Martin Garbade, Andres Milioto, Jan Quenzel, Sven Behnke, Cyrill Stachniss, and Jurgen Gall. SemanticKITTI: A dataset for semantic scene understanding of LiDAR sequences. In *ICCV*, pages 9297–9307, 2019.
- [11] Xiaoyu Tian, Tao Jiang, Longfei Yun, Yucheng Mao, Huitong Yang, Yue Wang, Yilun Wang, and Hang Zhao. Occ3D: A large-scale 3D occupancy prediction benchmark for autonomous driving. In *NeurIPS*, volume 36, 2024.
- [12] Xiaofeng Wang, Zheng Zhu, Wenbo Xu, Yunpeng Zhang, Yi Wei, Xu Chi, Yun Ye, Dalong Du, Jiwen Lu, and Xingang Wang. OpenOccupancy: A large scale benchmark for surrounding semantic occupancy perception. In *ICCV*, 2023.
- [13] Yi Wei, Linqing Zhao, Wenzhao Zheng, Zheng Zhu, Jie Zhou, and Jiwen Lu. SurroundOcc: Multi-camera 3D occupancy prediction for autonomous driving. In *ICCV*, 2023.
- [14] Wenzhao Zheng, Weiliang Chen, Yuanhui Huang, Borui Zhang, Yueqi Duan, and Jiwen Lu. OccWorld: Learning a 3D occupancy world model for autonomous driving. *arXiv preprint arXiv:2311.16038*, 2023.
- [15] Yihan Hu, Jiazhi Yang, Li Chen, Keyu Li, Chonghao Sima, Xizhou Zhu, Siqi Chai, Senyao Du, Tianwei Lin, Wenhai Wang, et al. Planning-oriented autonomous driving. In *CVPR*, pages 17853–17862, 2023.
- [16] Stefano V Albrecht, Cillian Brewitt, John Wilhelm, Balint Gyevnar, Francisco Eiras, Mihai Dobre, and Subramanian Ramamoorthy. Interpretable goal-based prediction and planning for autonomous driving. In *ICRA*, pages 1043–1049, 2021.
- [17] Giorgio Fumera and Fabio Roli. Support vector machines with embedded reject option. In *Pattern Recognition with Support Vector Machines: First International Workshop*, pages 68–82, 2002.
- [18] Dan Hendrycks, Kevin Zhao, Steven Basart, Jacob Steinhardt, and Dawn Song. Natural adversarial examples. In *CVPR*, pages 15262–15271, 2021.
- [19] Andrey Malinin, Bruno Mlodozieniec, and Mark Gales. Ensemble distribution distillation. In *ICLR*, 2019.
- [20] Pau de Jorge, Riccardo Volpi, Philip HS Torr, and Grégory Rogez. Reliability in semantic segmentation: Are we on the right track? In *CVPR*, pages 7173–7182, 2023.
- [21] Alexandru Niculescu-Mizil and Rich Caruana. Predicting good probabilities with supervised learning. In *ICML*, pages 625–632, 2005.
- [22] Chuan Guo, Geoff Pleiss, Yu Sun, and Kilian Q Weinberger. On calibration of modern neural networks. In *ICML*, pages 1321–1330. PMLR, 2017.

- [23] Shuran Song, Fisher Yu, Andy Zeng, Angel X Chang, Manolis Savva, and Thomas Funkhouser. Semantic scene completion from a single depth image. In *CVPR*, pages 1746–1754, 2017.
- [24] Mahdi Pakdaman Naeini, Gregory Cooper, and Milos Hauskrecht. Obtaining well calibrated probabilities using bayesian binning. In *AAAI*, 2015.
- [25] Levin Tishby and Solla. Consistent inference of probabilities in layered networks: predictions and generalizations. In *IJCNN*, pages 403–409, 1989.
- [26] John Denker and Yann LeCun. Transforming neural-net output levels to probability distributions. In *NIPS*, volume 3, 1990.
- [27] Yarín Gal and Zoubin Ghahramani. Dropout as a bayesian approximation: Representing model uncertainty in deep learning. In *ICML*, pages 1050–1059, 2016.
- [28] Xinlei Zhou, Han Liu, Farhad Pourpanah, Tiejong Zeng, and Xizhao Wang. A survey on epistemic (model) uncertainty in supervised learning: Recent advances and applications. *Neurocomputing*, 489:449–465, 2022.
- [29] Alain Jungo and Mauricio Reyes. Assessing reliability and challenges of uncertainty estimations for medical image segmentation. In *MICCAI*, pages 48–56, 2019.
- [30] Eyke Hüllermeier and Willem Waegeman. Aleatoric and epistemic uncertainty in machine learning: An introduction to concepts and methods. *Machine learning*, 110(3):457–506, 2021.
- [31] Alex Kendall and Yarín Gal. What uncertainties do we need in bayesian deep learning for computer vision? In *NIPS*, volume 30, 2017.
- [32] Diederik P Kingma and Max Welling. Auto-encoding variational bayes. *arXiv preprint arXiv:1312.6114*, 2013.
- [33] Jie Chang, Zhonghao Lan, Changmao Cheng, and Yichen Wei. Data uncertainty learning in face recognition. In *CVPR*, pages 5710–5719, 2020.
- [34] Meelis Kull, Miquel Perello Nieto, Markus Kängsepp, Telmo Silva Filho, Hao Song, and Peter Flach. Beyond temperature scaling: Obtaining well-calibrated multi-class probabilities with dirichlet calibration. In *NeurIPS*, volume 32, 2019.
- [35] Xingchen Ma and Matthew B. Blaschko. Meta-cal: Well-controlled post-hoc calibration by ranking. In *ICML*, pages 7235–7245, 2021.
- [36] Lingdong Kong, Xiang Xu, Jun Cen, Wenwei Zhang, Liang Pan, Kai Chen, and Ziwei Liu. Calib3d: Calibrating model preferences for reliable 3d scene understanding. *arXiv preprint arXiv:2403.17010*, 2024.
- [37] Hongyi Zhang, Moustapha Cisse, Yann N Dauphin, and David Lopez-Paz. mixup: Beyond empirical risk minimization. In *International Conference on Learning Representations*, 2018.
- [38] Andreas Geiger, Philip Lenz, and Raquel Urtasun. Are we ready for autonomous driving? The KITTI vision benchmark suite. In *CVPR*, pages 3354–3361, 2012.
- [39] Jianbiao Mei, Yu Yang, Mengmeng Wang, Tianxin Huang, Xuemeng Yang, and Yong Liu. SSC-RS: Elevate LiDAR semantic scene completion with representation separation and BEV fusion. In *IROS*, 2023.
- [40] Borui Zhao, Quan Cui, Renjie Song, Yiyu Qiu, and Jiajun Liang. Decoupled knowledge distillation. In *CVPR*, pages 11953–11962, 2022.
- [41] Morris H DeGroot and Stephen E Fienberg. The comparison and evaluation of forecasters. *Journal of the Royal Statistical Society: Series D (The Statistician)*, 32(1-2):12–22, 1983.
- [42] Yinpeng Dong, Caixin Kang, Jinlai Zhang, Zijian Zhu, Yikai Wang, Xiao Yang, Hang Su, Xingxing Wei, and Jun Zhu. Benchmarking robustness of 3d object detection to common corruptions. In *CVPR*, pages 1022–1032, 2023.
- [43] Shice Liu, Yu Hu, Yiming Zeng, Qiankun Tang, Beibei Jin, Yinhe Han, and Xiaowei Li. See and think: Disentangling semantic scene completion. In *NeurIPS*, volume 31, 2018.
- [44] Siqi Li, Changqing Zou, Yipeng Li, Xibin Zhao, and Yue Gao. Attention-based multi-modal fusion network for semantic scene completion. In *AAAI*, pages 11402–11409, 2020.
- [45] Yingjie Cai, Xuesong Chen, Chao Zhang, Kwan-Yee Lin, Xiaogang Wang, and Hongsheng Li. Semantic scene completion via integrating instances and scene in-the-loop. In *CVPR*, pages 324–333, 2021.
- [46] Jiayang Tang, Xiaokang Chen, Jingbo Wang, and Gang Zeng. Not all voxels are equal: Semantic scene completion from the point-voxel perspective. In *AAAI*, pages 2352–2360, 2022.
- [47] Joey Wilson, Jingyu Song, Yuewei Fu, Arthur Zhang, Andrew Capodieci, Paramsothy Jayakumar, Kira Barton, and Maani Ghaffari. Motionsc: Data set and network for real-time semantic mapping in dynamic environments. *IEEE RA-L*, 7(3):8439–8446, 2022.

- [48] Christoph B Rist, David Emmerichs, MarkusENZweiler, and Dariu M Gavrilă. Semantic scene completion using local deep implicit functions on LiDAR data. *TPAMI*, 2022.
- [49] Xuemeng Yang, Hao Zou, Xin Kong, Tianxin Huang, Yong Liu, Wanlong Li, Feng Wen, and Hongbo Zhang. Semantic segmentation-assisted scene completion for LiDAR point clouds. In *IROS*, 2021.
- [50] Sicheng Zuo, Wenzhao Zheng, Yuanhui Huang, Jie Zhou, and Jiwen Lu. PointOcc: Cylindrical tri-perspective view for point-based 3D semantic occupancy prediction. *arXiv preprint arXiv:2308.16896*, 2023.
- [51] Yuhang Lu, Xinge Zhu, Tai Wang, and Yuexin Ma. OctreeOcc: Efficient and multi-granularity occupancy prediction using octree queries. *arXiv preprint arXiv:2312.03774*, 2023.
- [52] Haoyi Jiang, Tianheng Cheng, Naiyu Gao, Haoyang Zhang, Wenyu Liu, and Xinggang Wang. Symphonize 3D semantic scene completion with contextual instance queries. In *CVPR*, 2024.
- [53] Zichen Yu, Changyong Shu, Jiajun Deng, Kangjie Lu, Zongdai Liu, Jiangyong Yu, Dawei Yang, Hui Li, and Yan Chen. FlashOcc: Fast and memory-efficient occupancy prediction via channel-to-height plugin. *arXiv preprint arXiv:2311.12058*, 2023.
- [54] Zhiqi Li, Zhiding Yu, David Austin, Mingsheng Fang, Shiyi Lan, Jan Kautz, and Jose M Alvarez. FB-OCC: 3D occupancy prediction based on forward-backward view transformation. *arXiv preprint arXiv:2307.01492*, 2023.
- [55] Yuqi Wang, Yuntao Chen, Xingyu Liao, Lue Fan, and Zhaoxiang Zhang. PanoOcc: Unified occupancy representation for camera-based 3D panoptic segmentation. *arXiv preprint arXiv:2306.10013*, 2023.
- [56] Chuandong Lyu, Shengbang Guo, Bin Zhou, Hailiang Xiong, and Hongchao Zhou. 3DOPFormer: 3D occupancy perception from multi-camera images with directional and distance enhancement. *T-IV*, 2023.
- [57] Junyi Ma, Xieyuanli Chen, Jiawei Huang, Jingyi Xu, Zhen Luo, Jintao Xu, Weihao Gu, Rui Ai, and Hesheng Wang. Cam4DOcc: Benchmark for camera-only 4D occupancy forecasting in autonomous driving applications. In *CVPR*, 2024.
- [58] Song Wang, Jiawei Yu, Wentong Li, Wenyu Liu, Xiaolu Liu, Junbo Chen, and Jianke Zhu. Not all voxels are equal: Hardness-aware semantic scene completion with self-distillation. In *CVPR*, 2024.
- [59] Bohan Li, Yasheng Sun, Xin Jin, Wenjun Zeng, Zheng Zhu, Xiaofeng Wang, Yunpeng Zhang, James Okae, Hang Xiao, and Dalong Du. Stereoscene: Bev-assisted stereo matching empowers 3d semantic scene completion. *arXiv preprint arXiv:2303.13959*, 2023.
- [60] Song Wang, Jiawei Yu, Wentong Li, Hao Shi, Kailun Yang, Junbo Chen, and Jianke Zhu. Label-efficient semantic scene completion with scribble annotations. In *IJCAI*, 2024.
- [61] Hao Shi, Song Wang, Jiaming Zhang, Xiaoting Yin, Zhongdao Wang, Zhijian Zhao, Guangming Wang, Jianke Zhu, Kailun Yang, and Kaiwei Wang. Occfiner: Offboard occupancy refinement with hybrid propagation. *arXiv preprint arXiv:2403.08504*, 2024.
- [62] Pin Tang, Zhongdao Wang, Guoqing Wang, Jilai Zheng, Xiangxuan Ren, Bailan Feng, and Chao Ma. Sparseocc: Rethinking sparse latent representation for vision-based semantic occupancy prediction. In *CVPR*, pages 15035–15044, 2024.
- [63] Guoqing Wang, Zhongdao Wang, Pin Tang, Jilai Zheng, Xiangxuan Ren, Bailan Feng, and Chao Ma. Occgen: Generative multi-modal 3d occupancy prediction for autonomous driving. In *ECCV*, 2024.
- [64] Jilai Zheng, Pin Tang, Zhongdao Wang, Guoqing Wang, Xiangxuan Ren, Bailan Feng, and Chao Ma. VEON: vocabulary-enhanced occupancy prediction. In *ECCV*, 2024.
- [65] Alex Kendall, Yarin Gal, and Roberto Cipolla. Multi-task learning using uncertainty to weigh losses for scene geometry and semantics. In *CVPR*, pages 7482–7491, 2018.
- [66] Yong Xu, Xiaozhao Fang, Xuelong Li, Jiang Yang, Jane You, Hong Liu, and Shaohua Teng. Data uncertainty in face recognition. *IEEE transactions on cybernetics*, 44(10):1950–1961, 2014.
- [67] Yuhang Zhang, Chengrui Wang, and Weihong Deng. Relative uncertainty learning for facial expression recognition. In *NeurIPS*, volume 34, pages 17616–17627, 2021.
- [68] Sixue Gong, Vishnu Naresh Boddeti, and Anil K Jain. On the capacity of face representation. *arXiv preprint arXiv:1709.10433*, 2017.
- [69] Salman Khan, Munawar Hayat, Syed Waqas Zamir, Jianbing Shen, and Ling Shao. Striking the right balance with uncertainty. In *CVPR*, pages 103–112, 2019.
- [70] Zhaopeng Dou, Zhongdao Wang, Weihua Chen, Yali Li, and Shengjin Wang. Reliability-aware prediction via uncertainty learning for person image retrieval. In *ECCV*, volume 13674, pages 588–605, 2022.
- [71] Kaiwen Cai, Chris Xiaoxuan Lu, and Xiaowei Huang. Uncertainty estimation for 3d dense prediction via cross-point embeddings. *IEEE RA-L*, 8(5):2558–2565, 2023.

- [72] Balaji Lakshminarayanan, Alexander Pritzel, and Charles Blundell. Simple and scalable predictive uncertainty estimation using deep ensembles. In *NIPS*, volume 30, 2017.
- [73] Roger W Johnson. An introduction to the bootstrap. *Teaching statistics*, 23(2):49–54, 2001.
- [74] Leo Breiman. Bagging predictors. *Machine learning*, 24:123–140, 1996.
- [75] Juozas Vaicenavicius, David Widmann, Carl Andersson, Fredrik Lindsten, Jacob Roll, and Thomas Schön. Evaluating model calibration in classification. In *AISTATS*, pages 3459–3467. PMLR, 2019.
- [76] Fabian Kupperts, Jan Kronenberger, Amirhossein Shantia, and Anselm Haselhoff. Multivariate confidence calibration for object detection. In *CVPRW*, pages 326–327, 2020.
- [77] Muhammad Akhtar Munir, Muhammad Haris Khan, M. Sarfraz, and Mohsen Ali. Towards improving calibration in object detection under domain shift. In *NeurIPS*, volume 35, pages 38706–38718, 2022.
- [78] Kemal Oksuz, Tom Joy, and Puneet K. Dokania. Towards building self-aware object detectors via reliable uncertainty quantification and calibration. In *CVPR*, pages 9263–9274, 2023.
- [79] Teodora Popordanoska, Aleksei Tiulpin, and Matthew B. Blaschko. Beyond classification: Definition and density-based estimation of calibration in object detection. In *WACV*, pages 585–594, 2024.
- [80] Zhipeng Ding, Xu Han, Peirong Liu, and Marc Niethammer. Local temperature scaling for probability calibration. In *ICCV*, pages 6889–6899, 2021.
- [81] Elias Kassapis, Georgi Dikov, Deepak K. Gupta, and Cedric Nugteren. Calibrated adversarial refinement for stochastic semantic segmentation. In *ICCV*, pages 7057–7067, 2021.
- [82] Dongdong Wang, Boqing Gong, and Liqiang Wang. On calibrating semantic segmentation models: Analyses and an algorithm. In *CVPR*, pages 23652–23662, 2023.
- [83] Kaiming He, Xiangyu Zhang, Shaoqing Ren, and Jian Sun. Deep residual learning for image recognition. In *CVPR*, pages 770–778, 2016.

Supplemental Material

In this part, we further provide more details, additional experimental results and discussions on our proposed approach:

- §A: More implementation details;
- §B: Additional experiments;
- §C: Further discussions;
- §D: License and consent with public resources.

A More Implementation Details

A.1 Online Uncertainty Learning

VoxFormer Framework. VoxFormer [5] is a two-stage semantic occupancy prediction model with a highly efficient design. To simplify the problem, we use the results of the Stage-I (Class-Agnostic Query Proposal) provided by the official checkpoint. Then we retrain the model by incorporating uncertainty learning in the more important Stage-II (Class-Specific Segmentation). The vision encoder uses ResNet-50 [83] as backbone. The primary loss \mathcal{L}_{occ} in VoxFormer consists of the weighted cross entropy loss and scene-class affinity losses on both geometry and semantics from MonoScene [3]. All the models with online uncertainty estimation have been trained with a learning rate of $2e^{-4}$ and a batch size of 1 per GPU for 20 epochs.

SGN Framework. SGN is an end-to-end framework with a “dense-sparse-dense” design, which introduces hybrid guidance and effective voxel aggregation. The ResNet-50 [83] is also adopted as vision backbone. The 2D-to-3D transformation is similar to MonoScene [3]. In addition to the loss from VoxFormer, \mathcal{L}_{occ} in SGN also includes geometric and semantic guidance losses specially designed for the “dense-sparse-dense” structure. The related models with online uncertainty estimation are trained with a learning rate of $2e^{-4}$ and a batch size of 1 per GPU for 40 epochs.

A.2 Offline Model Calibration

In our offline setting, the parameters of the original occupancy network are entirely frozen, with only the parameters in the calibration function and uncertainty learning module being trainable. For the implementation of DeptS in the occupancy network, we calculate the coordinates and depth of the voxel centers to replace the depth of the point cloud used in the original code⁴. We adopt a simple log-likelihood loss for \mathcal{L}_{calib} .

B Additional Experiments

B.1 Qualitative Comparison

We further provide evaluation results on *class-agnostic* geometric metrics from our robustness analysis experiments (see §5.3) in Figure A1. Under four different out-of-domain perturbations, our method demonstrates superior geometric reliability (PRR_{geo} and ECE_{geo}) compared to SGN [9] and shows significant advantages in accuracy (IoU).

B.2 Qualitative Comparison

Online Uncertainty Learning. We present more error maps with uncertainty maps from the predictions of SGN [9] and RELIOCC under the online setting. As shown in the left column of Figure A3, SGN exhibits low uncertainty in many parts of the scene where it makes incorrect predictions, indicating a severe issue of over-confidence. In contrast, in the right column of Figure A3, our method demonstrates high uncertainty in most of the incorrect prediction areas, further illustrating that RELIOCC effectively addresses the problem of over-confidence and improves model reliability.

Offline Model Calibration More reliability diagrams of the predictions on the validation set of SemanticKITTI are presented in Figure A2. In various scenarios, our uncertainty-aware calibration

⁴<https://github.com/ldkong1205/Calib3D>

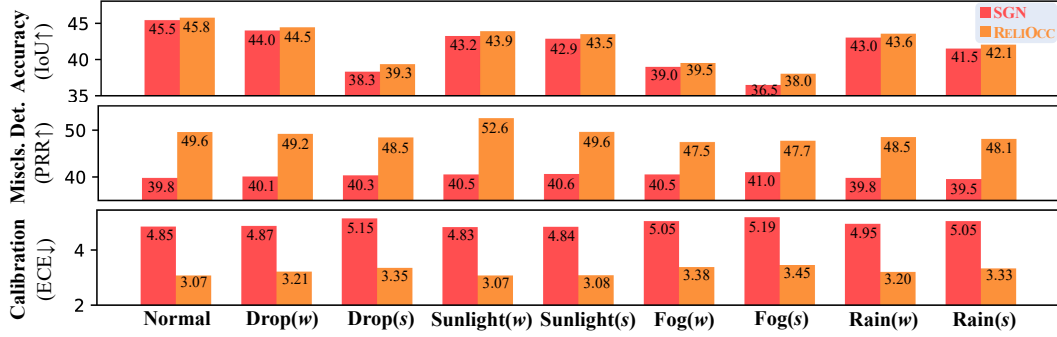


Figure A1: The geometric comparison in accuracy and reliability performance between SGN [9] and RELIOCC under four out-of-domain conditions.

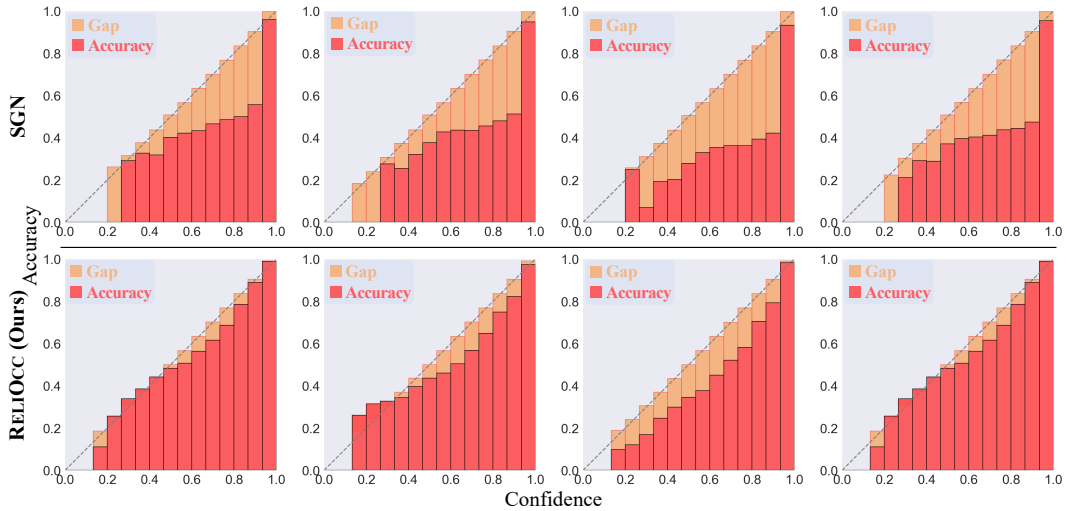


Figure A2: More reliability diagrams of semantic calibration gaps in randomly selected predictions from SGN [9] and RELIOCC.

strategy effectively reduces calibration gap compared to the SGN [9], providing more reliable semantic occupancy prediction results.

C Further Discussions

C.1 Limitation and Future Work

Although our method has achieved significant improvements in reliability metrics for camera-based occupancy models, even approaching the performance of some LiDAR-based methods [7, 2] in PRR and ECE, we cannot ignore the accuracy gap (mIoU and IoU) between camera and LiDAR. Therefore, camera-based models still have a long way to go. In the future, we will explore using the learned uncertainty in camera to promote label accuracy in offline annotation, reducing reliance on LiDAR and contributing a data loop for a purely vision-based occupancy network.

C.2 Potential Societal Impact

Our work explores and enhances the reliability of vision-based occupancy networks, which can significantly improve the safety and accessibility of autonomous driving systems with low-cost sensors. This advancement not only fosters safer navigation and decision-making in autonomous vehicles but also promotes wider adoption of affordable and reliable AI technologies in various applications, contributing positively to transportation efficiency and public safety. Conversely, the widespread utilization of sensors in autonomous vehicles raises apprehensions regarding data privacy and security. The formulation of robust data storage and management strategies becomes imperative.

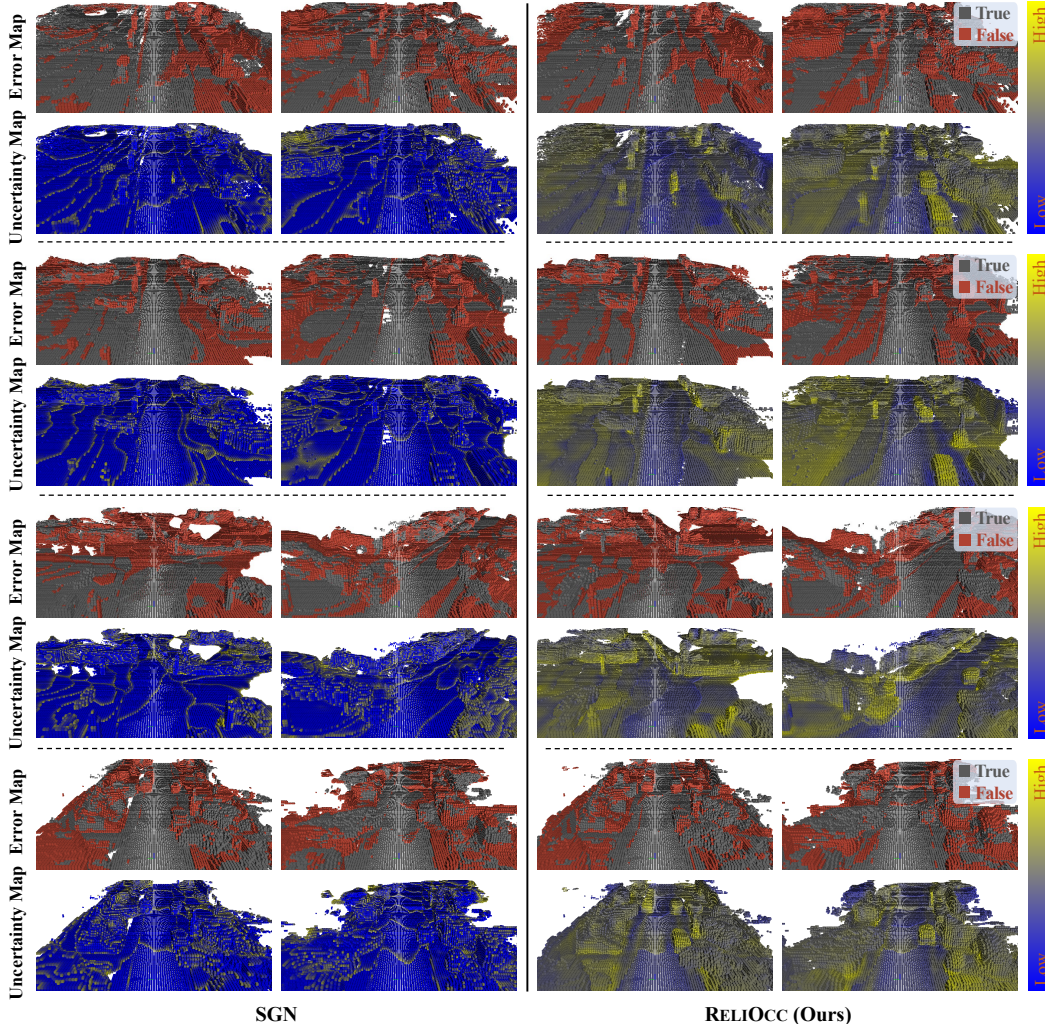


Figure A3: More visual results of the error map and corresponding uncertainty map from the predictions by SGN [9] and RELIOCC.

D License and Consent with Public Resources

D.1 Public Datasets

We use the semantic scene completion annotations provided by the SemanticKITTI dataset and the original image data from the KITTI Odometry Benchmark:

- SemanticKITTI⁵ CC BY-NC-SA 4.0
- SemanticKITTI-API⁶ MIT License
- KITTI Odometry Benchmark⁷ CC BY-NC-SA 3.0

D.2 Re-evaluated Methods

In the experimental section, we evaluated 10 existing semantic occupancy prediction models, all reproduced using the official code:

⁵<http://semantic-kitti.org>.
⁶<https://github.com/PRBonn/semantic-kitti-api>.
⁷https://www.cvlibs.net/datasets/kitti/eval_odometry.php.

- SSCNet⁸ MIT License
- LMSCNet⁹ Apache License 2.0
- JS3C-Net¹⁰ MIT License
- SSC-RS¹¹ MIT License
- SCPNet¹² Unknown
- MonoScene¹³ Apache License 2.0
- TPVFormer¹⁴ Apache License 2.0
- VoxFormer¹⁵ NVIDIA Source Code License-NC
- NDCScene¹⁶ Unknown
- SGN¹⁷ Unknown

D.3 Other Resources

For the calculation of PRR and ECE metrics, the design of out-of-domain perturbations, and the plotting of reliability diagrams, we have referred to the following publicly available implementations for other tasks and made modifications specific to semantic occupancy prediction:

- relis¹⁸ CC BY-NC-SA 4.0
- 3D Corruptions AD¹⁹ MIT License
- reliability diagrams²⁰ MIT License

⁸<https://github.com/shurans/sscnet>.

⁹<https://github.com/astra-vision/LMSCNet>.

¹⁰<https://github.com/yanx27/JS3C-Net>.

¹¹<https://github.com/Jieqianyu/SSC-RS>.

¹²<https://github.com/SCPNet/Codes-for-SCPNet>.

¹³<https://github.com/astra-vision/MonoScene>.

¹⁴<https://github.com/wzzheng/tpvformer>.

¹⁵<https://github.com/NVlabs/VoxFormer>.

¹⁶<https://github.com/Jiawei-Yao0812/NDCScene>.

¹⁷<https://github.com/Jieqianyu/SGN>.

¹⁸<https://github.com/naver/relis>.

¹⁹https://github.com/thu-ml/3D_Corruptions_AD.

²⁰<https://github.com/hollance/reliability-diagrams>.